Unusual energy–structure–property relation in a metallic glass coupled with temperature-dependent relaxation memories

Masato Wakeda[1,*], Junji Saida[2]

[1]Research Center for Structural Materials, National Institute for Materials Science, 1-2-1 Sengen, Tsukuba, 305-0047, Japan

[2] Frontier Research Institute for Interdisciplinary Sciences, Tohoku University, 6-3 Aoba, Aramaki, Aoba-ku, Sendai, 980-8578, Japan

*WAKEDA.Masato@nims.go.jp

Keywords

Metallic glasses, Relaxation, Memory effect, Molecular dynamics, Supercooled liquid

Abstract

Elucidating the individual effects of high- and low-temperature relaxations on the internal structure and material properties is a fascinating theme in the field of metallic glasses because it can lay the foundation for an advanced glass-property tuning scheme through the control of different types of relaxations. In this study, several glass models were constructed using melt-quenching (MQ) processes, in which high- and low-temperature relaxations were controlled by their cooling rates. We found unusual energy–structure–property relationships; even when the glass alloys had equivalent potential energies (or free volumes), they exhibited different local-order development, elastic stiffness, and plastic deformation properties, which depended on the thermal histories in the glass-forming MQ process. The local-order development was primarily affected by the high-temperature relaxation occurring at approximately the glass transition temperature. Meanwhile, the plastic deformation behavior of the metallic glasses was significantly affected by both low- and high-temperature relaxations. We also found an interesting relaxation memory effect in the glass alloys constructed by the present MQ processes; the glass alloys exhibited an atomic-scale dynamic that was affected by the temperature-dependent relaxation memories (i.e., high and- low-temperature relaxation memories) of previous MQ

processes. These results provide new insights into the relaxation physics of glass-forming liquids and imply the possibility of an advanced tuning scheme for metallic glasses.

1. Introduction

Metallic glasses lack long-range ordered structures and exhibit interesting properties such as soft magnetism, high corrosion resistance, and large elastic elongation [1,2,3,4]. Metallic glasses are generally prepared by rapid cooling from high-temperature melts using the melt-quenching (MQ) process [5,6,7]. In MQ processes, if the cooling rate is sufficiently high to avoid crystallization, alloys change their phase in the order of high-temperature liquid, supercooled liquid (i.e., liquid below the melting temperature), and glass solid below the glass transition temperature, T_g. In general, supercooled liquids and glass solids exhibit relaxation behaviors [8]. By the relaxation, glassy alloys become energetically more stable and have higher-density states (i.e., smaller free-volume states). For the past decades, various studies on relaxation in supercooled liquid alloys and glass alloys have been conducted [9,10,11]. For instance, different types of relaxations have been observed, such as α- and β-relaxations [11,12,13]. In dynamical mechanical spectrum, the peak corresponding to α-relaxation is observed around T_g, whereas the peak corresponding to β-relaxation is often observed at a lower temperature than that reported for α-relaxation [13,14,15]. The relaxations are significantly correlated with the nature of nonequilibrium glass [16,17,18] and affect the material properties of metallic glasses, such as elastic stiffness and plastic deformability [11]. Therefore, a deeper understanding of both the relaxation physics in the MQ process and thermal processing for controlling material properties is still required. Conventional experimental and atomistic studies have discussed the effects of cooling rate on potential energy, free volume, characteristic local order, elastic constant, and plastic deformation [11,19,20]. A lower cooling rate reduces enthalpy and free volume throughout the cooling process. Meanwhile, supercooled liquids and glass solids have different types of relaxation with different timescales. Therefore, the effect of cooling rate on the properties of metallic glasses during the quenching process possibly differs depending on the temperature and relaxation timescale [21]. In other words, more sophisticated approaches to property tuning by individual or selective control of different types of relaxation must exist.

This molecular dynamics (MD) study reveals an unusual energy–structure–property relation generated by controlling temperature-dependent relaxations in MQ processes. Simple binary model systems with pairwise interatomic interactions were used to provide a basic and general discussion of the relaxation physics applied to wide glass-alloy systems. Although the relaxation phenomena observed in the present binary system are relatively simple, we reveal complex effects of the relaxations on the energy, structure, and properties. To control relaxation

in the MQ process, we employed two-step MQ simulations, in which the cooling rate changes at around T_g in the MQ process. In conventional atomistic simulations, even when the effect of the cooling rate was discussed, the cooling rate remained constant throughout the MQ process. Therefore, the individual or separate effects of different types of relaxation in the MQ process have not been considered in both experimental and computational quenching studies. In our previous study [21], we changed the cooling rate in the cooling process from a high temperature to a low temperature and discussed the critical temperature range over which the cooling rates affect the final glass state. Because such a complex cooling-rate control remains challenging in the experimental MQ process, atomistic simulations can be used to provide a deeper understanding of the relaxation phenomena beyond the experiments. In the two-step MQ simulations, we selectively controlled the degree of high- and low-temperature relaxations by changing the cooling rate. Thus, the two-step MQ process enables us to realize glass models that underwent tuned relaxation histories: case (A) slow cooling at high temperatures and fast cooling at low temperatures; case (B) fast cooling at high temperatures and slow cooling at low temperatures. Analyses of the internal structure, dynamical properties, and plastic deformation behavior of the constructed glass models revealed unusual energy–structure–property relationships realized by controlling high- and low-temperature relaxations. We also observed that the memory effects of temperature-dependent relaxation in dynamical mechanical analysis correlated with the existence of relaxations with different energy barriers and heterogeneous microstructures. These results suggest new aspects of relaxation physics in MQ processes and an advanced approach to tuning glass properties by controlling high- and low-temperature relaxations.

2. Material and methods

In this study, we used the $Cu_{50}Zr_{50}$ binary model alloys. Similar to our previous studies on Cu-Zr alloys [22,23,24], here, we aimed to reveal the general physics of glass alloys and obtain useful knowledge for improving the material properties of wide metallic-glass systems rather than obtain realistic material properties of specific Cu-Zr alloys. Therefore, simple binary alloys and pairwise potentials [25,26] were used to maintain the generality of the discussion. The knowledge obtained will be useful for wide metallic glass systems with dense random packing features. The number of atoms in the model was 30,000. The LAMMPS code [27] was used for MD simulations. In all the MQ processes, an isothermal–isobaric ensemble was applied. For the models constructed using the MQ processes, MD-DMA simulations were conducted at various temperatures by applying shear strain of $\gamma^* \sin(2\pi t/t^*)$, where t is time ($\gamma^* = 0.02$ and $t^* = 1000$ ps) [24,28,29]. We applied ten cycles in each DMA calculation. In the DMA calculations, we evaluated the atomic

displacement Δr during one period of the DMA sinusoidal cycle. The histogram of Δr is obtained by the normalized probability density function $p(\Delta r)$ [30]. For the models obtained using the MQ processes, simple shear simulations were conducted by gradually increasing a shear strain component. The shear-strain rate was set to 10^8 s^{-1}. The temperature was set to 10 K and remained constant during the shear simulations. The local atomic displacements (used in f_D analysis) were calculated by the norm of $\boldsymbol{H}_0(\boldsymbol{s}-\boldsymbol{s}_0)$, excluding the applied homogeneous shear. $\boldsymbol{H}_0$ and $\boldsymbol{s}_0$ are a cell-matrix and a normalized atomic position at a shear strain of 0.0, while $\boldsymbol{s}$ is a normalized atomic position at a shear strain of 0.05. In the MQ, DMA, and shear simulations, periodic boundary conditions were assigned in all orthogonal directions. To obtain statistical averages, we conducted ten independent MQ simulations for each quenching condition. This study also discusses the potential energy, volume, dynamical properties, elastic stiffness, and plastic deformations based on the averaged quantities. OVITO [31] was used to visualize the atomic configurations.

3. Results

First, we demonstrate the temperature-dependent relaxation features. The self-intermediate scattering function (SISF) at various temperatures from 1500 K to 700 K is shown in Fig. 1(a). T_g defined by a kink point of volume-temperature curve in the conventional MQ simulation (i.e., cooling rate is constant throughout the cooling process) at a cooling rate of 10^{11} K/s is approximately 860 K. In Fig. 1(a), we can observe a monotonic relaxation from 1.0 to 0 at temperatures exceeding 1100 K within a short period of 10^{-10} s. Meanwhile, at 1000 K, the SISF has a small shoulder, and the relaxation timescale is extended. Below 900 K, the SISF immediately decreases from 1.0 to approximately 0.7-0.8 and then exhibits an almost constant region. Then, the SISF decreases again from approximately 0.7-0.8 to 0. As schematically shown in Fig. 1(b), various atomistic studies have reported on these two-stage relaxation [18]. At approximately T_g, α-relaxation is the dominant phenomenon in experiments. At lower temperatures, β-relaxation emerges as another significant phenomenon in metallic glasses [32]. Notably, the temperature ranges of α- and β-relaxations cannot be completely separated because a part of these ranges overlap each other [18]. At temperatures above T_g, sufficient relaxation can occur within the MD timescale, as shown in the curves of 1500–1100 K in Fig. 1(a). Then, as the temperature decreased further, the relaxation timescale increased significantly. Within the range of 900–700 K in Fig. 1(a), SISFs exhibit a small reduction at approximately 10^{-13} s and then remained almost constant. The origin of this constant region (i.e., the plateau region) has been discussed based on atomistic cages, in which atoms are trapped transitionally (fast β-relaxation). Then, a sufficiently long time enables cage-breaking of the atoms, and full relaxation occurs [11,13].

Because the degree of relaxations occurring in MQ processes is significantly affected by the quenching timescale, the appropriate control of the cooling rate in the MQ process can change the degree of relaxation. We show the schematic of "one-step" and "two-step" MQ processes in Fig. 2(a). In the one-step MQ process (i.e., conventional cooling process used in atomistic simulations), we conducted an MQ simulation with constant cooling rates from 2000 K to 0 K. Five different cooling rates of $Q_1 = 10^{10}$, 3×10^{10}, 10^{11}, 3×10^{11}, and 10^{12} K/s were used. The glass models constructed by the one-step MQ processes are named as "(I)10^{10}," "(I)3×10^{10}," "(I)10^{11}," "(I)3×10^{11}," and "(I)10^{12}", where "(I)" denotes the one-step MQ process. In conventional MD studies, the cooling rate is kept constant throughout the cooling process. Meanwhile, in the two-step MQ from 2000 K to 0 K, we changed the cooling rate at κ [K] (II-A) from a slow cooling rate (Q_{2s}) to a fast cooling rate (Q_{2f}), and (II-B) from a fast cooling rate (Q_{2f}) to a slow cooling rate (Q_{2s}). Here "(II)" denotes the two-step MQ processes. We used $Q_{2f} = 10^{12}$ K/s and $Q_{2s} = 10^{10}$ K/s. The models constructed by the two-step MQ processes are denoted by "(II-A)κ" and "(II-B)κ;". We constructed "(II-A)800," "(II-A)900," "(II-A)950," and "(II-A)1000" for (II-A) and "(II-B)700," "(II-B)800," "(II-B)850," "(II-B)900," and "(II-B)1000" for (II-B). In all of the MQ processes, the alloy models at 2000 K are high-temperature liquids, whereas the models become glass solids at 0 K because of the glass transition in the MQ processes. In this study, no clear crystallization was observed in any of the constructed models. A slower cooling rate generally enables a glass solid to achieve a well-relaxed state. Therefore, the glass models constructed using the two-step method (II-A)κ have a relatively larger degree of relaxation in the high-temperature range and a smaller degree of relaxation in the low-temperature range than the glass model constructed by the two-step method (II-B)κ.

Figure 2(b) shows the relationship between the volume and potential energy of all the constructed models. A slower cooling rate leads to a lower potential energy and smaller volume owing to a large degree of relaxation, and vice versa [33,34]. This well-known trend is valid in Fig. 2(b); for instance, one-step MQs with $Q_1 = 10^{12}$ K/s and $Q_1 = 10^{10}$ K/s have the highest and lowest potential energies (and the largest and smallest volumes) among all the models, respectively. In addition, in Fig. 2(b), the plots of one-step and two-step MQ processes have the same linear correlation, suggesting that the two-step MQ method does not change the potential energy–volume relation of the conventional one-step MQ method in this model system.

Meanwhile, we observed an unusual trend in the potential energy–internal structure correlation. Figure 3 shows the effects of high- and low-temperature relaxations on the formation of icosahedral short-range order (I-SRO) and medium-range order (I-MRO) [22]. I-SRO and I-MRO, as shown in Fig. 3(a), are well-known local orders that are discussed in terms of glass-forming ability, local plastic deformation, and structural heterogeneity [23,35]. I-MRO is defined by the cluster composed of interpenetrating I-SROs. Here we evaluated the clustering coefficient

of I-MRO, representing the degree of development of I-MRO. The clustering coefficient for the center atom of an icosahedron is expressed as $2L_a/n_B(n_B-1)$; L_a and n_B are the number of triangular geometry composed of interpenetrating icosahedra and the interpenetrating icosahedral number, respectively. Here, the triangular unit is the basis of clustering [22]. The statistical average of the clustering coefficients for all icosahedra was used for analysis. The larger the clustering coefficient, the more developed the I-MRO in the model, and vice versa. Figures 3(b) and 3(c) show the fractions of I-SRO and I-MRO as a function of the potential energy. In Fig. 3, glass models with developed icosahedral local orders have low potential energies, and vice versa [20]. Furthermore, we observe beyond one-to-one correlations between I-SRO and potential energy and between I-MRO and potential energy. For instance, if the two glass models have similar potential energies (or free volumes), they exhibit different local order development (i.e., I-SRO and I-MRO). The two-step (II-A) line exhibits a higher fraction, while the two-step (II-B) line exhibits a lower fraction of I-SRO and I-MRO. The result shown in Fig. 3 can be explained based on the existence of relaxations with different effects on the local orders and potential energy (or free volume). Although these relaxations reduce the potential energy and increase the I-SRO and I-MRO, one relaxation has a larger effect than another on the formation of the local orders. The evolution of the relationship between the fraction of I-SRO and potential energy during MQ is also shown in Fig. S1 in Supplementary Material.

We additionally found characteristic dynamics in the dynamic mechanical analysis (DMA) simulations. The obtained results suggest that the glass models constructed using the present MQ processes memorize the temperature-dependent relaxations that occurred in the previous MQ processes. Figure 4 shows the effect of high- and low-temperature relaxations on the dynamic properties of glass models constructed by the MQ processes. We conducted MD-DMA analyses at various temperatures and obtained the average atomic displacement, Δr of the model. Figure 4(a) shows the average Δr differentiated from that of the one-step 10^{10} K/s model, which should have the lowest potential energy, smallest free volume, and smallest Δr at all temperatures. All curves exhibit a similar trend; the difference in average Δr increases with increasing temperature, reaching a peak at around T_g. The peak height depends on the thermal history of the MQ process. In Fig. 2(b), the glass models of one-step ($Q_1 = 3 \times 10^{10}$ K/s), two-step A (κ = 900 K), and two-step B (κ = 900 K) (i.e., (I) 3×10^{10}, (II-A)900, and (II-B)900, respectively) have similar potential energies and volumes. Therefore, we focused on the three glass models. Notably, we cannot clearly distinguish among the three models based on the potential energies and volumes (i.e., macroscopic and static properties) at a low temperature. Figure 4(b) shows the difference in average Δr between (II-A)900 and (I)3×10^{10} and between (II-B)900 and (I)3×10^{10}, which indicates interesting temperature–dependent differences among the three models. For instance, the difference in the average Δr of (II-B)900 is smaller than that

of (I)3 × 10^{10} below 900 K, whereas this value is larger above 900 K. This result reflects the relaxation histories in the previous MQ process; the degree of relaxation of (II-B)900 is larger than that of (I)3 × 10^{10} below 900 K and smaller above 900 K owing to the cooling rates in the MQ process. The large relaxation in the previous MQ process suppresses atomic motion in the subsequent DMA simulations, whereas a small relaxation in the MQ allows further atomic motion in the subsequent DMA. A similar behavior is also observed in the difference in Δr between (II-A)900 and (I)3 × 10^{10}: the value of (II-A)900 is larger than that of (I)3 × 10^{10} below 800 K, whereas the value is smaller above 800 K. These results imply that the glass models constructed by the MQ process exhibit temperature-dependent dynamic behavior, which reflect the thermal histories in the preceding MQ process. In other words, glass models memorize histories of high- and low-temperature relaxations in the glass-forming MQ processes and exhibit temperature-dependent dynamic behavior depending on the thermal histories. The temperature–memory effect below the crystallization temperature was reported in a recent experimental study [36], in which glass models memorized the temperature at which deformation occurred in the previous thermomechanical process. Our observations show that the glass models can memorize the temperature-dependent relaxation histories in glass-forming MQ processes and exhibit dynamic behavior depending on the thermal histories.

DMA also provides information on the heterogeneous relaxation in the glass model. Figures 4(c) and 4(d) imply that temperature-dependent atomic motion and the internal structure of the glass models have heterogeneities. In a previous study [37], we revealed that the histogram of Δr obtained in the unfreezing process reflects the inherent structural heterogeneity in glass solids. At approximately T_g, the histogram has two peaks: the left peak corresponds to regions with small atomic mobility (or densely packed regions, or strongly bonded regions; SBR), while the right peak corresponds to regions with large atomic mobility (or loosely packed regions, or weakly bonded regions; WBR) [37,38,39]. Because I-SRO and I-MRO have higher packing densities than the average local structure, these icosahedral local orders mainly contribute to regions with low atomic mobility (or densely packed regions, or SBR). In Fig. 4(c), we compare the histograms of Δr between (II-A)800 and (I)10^{10} obtained by DMA simulations at 700, 800, 900, and 1000 K. The two models have similar histograms above 900 K but different histograms below 800 K. For the histograms at 700 K, the two models exhibit different shapes at the right peak (i.e., the large Δr region) but similar histogram shapes in the small Δr region. Figure 4(c) suggests that the difference in relaxation history between the two models affects the atomic mobility of the large Δr region (i.e., loosely packed regions or WBR). The two models have the same relaxation histories in the MQ processes above 800 K, and, thus, a similar internal topological order, as confirmed in Fig. 3 (see (II-A)800 and (I)10^{10}). Although the two models have similar development of I-SRO and I-MRO (i.e., high-density region or SBR), they have

different degrees of relaxation at low temperatures. The difference in Fig. 4(c) suggests that low-temperature relaxation affects the atomic mobility in the large Δr region (i.e., loosely packed regions, or WBR), in which (II-A)800 exhibits a larger fraction than (I)10^{10} at 700 and 800 K. This result suggests that the memory effects of the previous high- and low-temperature relaxations are correlated with their heterogeneous microstructures. The relaxation memory effects are also shown in Fig. 4(d), in which the histograms between (II-A)900 and (II-B)900 are compared. Although the two models have similar potential energies, they have different internal structures, as shown in Fig. 3. Figure 4(d) reveals the different atomic motion; below T_g, atomic motion mainly occurred in the loosely packed region (i.e., WBR) in the present DMA timescale. In the MQ processes, (II-A)900 had less relaxation than (II-B)900 below 900 K. Therefore, in the DMA simulation at 700 K, which is lower than T_g, we can observe a difference in the histogram between the two models in the large Δr region, that is, (II-A)900 is larger than (II-B)900. In DMA simulations at relatively high temperatures, such as T_g, unfreezing occurs even in the densely packed region (i.e., SBR) within the present DMA timescale. Therefore, a difference is observed in the small Δr region. In the MQ processes, (II-A)900 has a larger relaxation than (II-B)900 above 900 K; thus, (II-A)900 has more developed I-SRO and I-MRO than (II-B)900, as shown in Figs. 3(b) and 3(c). Therefore, in the DMA simulation at 1000 K, which is higher than T_g, (II-A)900 is more stable than (II-B)900 in the small Δr region. These results suggest that high- and low-temperature relaxation in MQ processes have spatially different effects on the Δr in the DMA simulations; high-temperature relaxation mainly affects the densely packed region (i.e., SBR), while low-temperature relaxation mainly affects the loosely packed regions (i.e., WBR). These results suggest that glass alloys memorize the relaxation temperature (or relaxation type) and relaxation heterogeneity in the MQ processes.

Figure 5 shows the shear simulations for the glass models constructed using various MQ processes. The two quantities are described in Figs. 5(b)–5(e). Here, we consider the shear modulus G and deformation ratio f_D (see Fig. 5(a)). The shear modulus was obtained from the shear stress vs. shear strain correlation with shear strain < 0.01. The deformation ratio, f_D, was obtained from the atomic configuration when the shear strain was 0.05, at which the glass model exhibited local plastic deformation. Based on the calculation of the local atomic displacement, the number of atoms having the local atomic displacement larger than 0.2 Å is evaluated and denoted by n_D. We selected 0.2 Å as the threshold value after comparing it to other values (see Fig. S2 in Supplementary Material). This value does not affect the qualitative trends obtained in this study. The deformation ratio is then evaluated using $f_D = n_D/N_A$ (N_A denotes the total number of atoms). Therefore, a large f_D indicates that glass models have a large degree of local plastic deformation region, and vice versa. Figures 5(b) and 5(c) represent G and f_D vs. the fraction of I-SRO, respectively. In the conventional discussion, a large fraction of I-SRO increases G and

decreases f_D [23]. Notably, this trend is valid in Figs. 5(b) and 5(c). However, the fraction of I-SRO or development of I-MRO is not a sufficient parameter in this study. Even if the fractions of I-SRO are identical, the glass model that undergoes large low-temperature relaxation has a larger G and smaller f_D. Figures 5(d) and 5(e) show G and f_D vs. potential energy, respectively. In Figs. 5(d) and 5(e), we can find differences in the G and f_D vs. potential energy correlation between the one-step, two-step (II-A), and two-step (II-B) MQ models. Two-step (II-A) and two-step (II-B) have relatively smaller and larger G values, respectively, even if their potential energies are similar. By contrast, two-step (II-A) and two-step (II-B) has larger and smaller f_D values even if their potential energies are similar. Figs. 5(c) and 5(e) show that both low-temperature and high-temperature relaxations significantly influence the plastic deformation behavior. An experimental DMA analysis indicates that β-relaxation increases the mechanical modulus [40]. In addition, previous experimental studies indicated that plastic deformation in metallic glass had similar energy barrier for β-relaxation because the local deformation at shear transformation zone (STZ) was similar to the β-relaxation [13,41]. Another experimental study indicated that α- and β-relaxations were both consistent with the STZ theory [42]. Figures 5(c) and 5(e) suggest that both high- and low-temperature relaxations affect the plastic deformation behavior of the present glass systems.

4. Discussions

We discuss the background physics of the findings obtained in the present study in Fig. 6. Figures 3 and 5 suggest that we can obtain two glass models with similar potential energies but different development of local orders (e.g., I-SRO and I-MRO), elastic stiffness, and plastic deformation behavior (denotes by "(1) unusual energy–structure–property relation" in Fig. 6). A recent MD study suggests that α- and β-relaxations can be observed within the MD timescale [29]. Since the cooling rate of 10^{10} K/s used in the present MD-MQ is sufficiently slow for the MD timescale, one possible explanation regarding the underlying physics behind the present findings (i.e., the unusual energy–structure–property relations and the relaxation memory effect) is associated with α- and β-relaxations. In this explanation, high- and low-temperature relaxations are mainly correlated with α- and β-relaxations, respectively. This explanation suggests that α- and β-relaxations have different energy barriers and different effects on the internal structures and glass properties. In contrast, it may be possible to consider them mainly based on α-relaxation; when α-relaxation occurs over a relatively wide temperature range [43], it can also explain the present results. In both explanations, the key point is the existence of relaxations with different energy barriers and different effects on the internal structures and glass properties. During MQ processes, these relaxations occur depending on the temperature and cooling rate. The two-step

MQ process changes the degree of relaxations by controlling the cooling rates in the high- and low-temperature regions. We obtained glass models exhibiting (A) high and low degrees of relaxation at high- and low-temperature ranges, respectively, and (B) low and high degrees of relaxation at high- and low-temperature ranges, respectively. For instance, the degree of relaxation of the models (I)3×10^{10}, (II-A)900, and (II-B)900 decreases in the order (II-A)900 > (I)3×10^{10} > (II-B)900 at a high-temperature range, whereas it increases in the order (II-A)900 < (I)3×10^{10} < (II-B)900 at a low-temperature range. Although both high- and low-temperature relaxations reduce the potential energy and free volume, their detailed effects on the development of local order, elastic stiffness, and plastic deformation behavior are different. In a recent experimental study, decoupling between enthalpy and mechanical properties in rejuvenated metallic glass was observed [44]. Moreover, experiments have been conducted to separate β-relaxation from α-relaxation in fragile metallic glasses based on ultrafast flash differential scanning calorimetry [45]. This study revealed the feasibility of controlling the degree of high- and low-temperature relaxations in a two-step MQ and their various effects on the internal structure and properties of glass. In other words, this study demonstrates the partial decoupling effects of high- and low-temperature relaxations on the structure and deformation properties of glass. We showed an unusual energy–structure–property relation, which suggests an advanced tuning of glass properties by controlling different types of relaxations. Notably, the relaxation timescale differs depending on the alloy composition. A key factor to control the relaxation state by the MQ process is the relationship between the relaxation timescale and cooling rate because the cooling rate can affect the relaxation phenomena when this rate has a timescale comparable to the relaxation timescale [21]. Therefore, one should appropriately choose the cooling rate at high- and low-temperature ranges depending on the alloy system to control each relaxation phenomenon.

In addition, our DMA simulations suggest that the glass models memorize the relaxation histories in the previous MQ processes, as indicated by "(2) memory effect of previous temperature-dependent relaxation" and shown in the lower left images in Fig. 6. In the conventional understanding, the energy landscape of a glassy system has different scale basins: large and small basins, which are related to high- and low-temperature relaxations, respectively [16,46]. High-temperature relaxations overcome higher energy barriers than low-temperature relaxations in both MQ (freezing) and DMA simulations (unfreezing). As discussed above, the two-step MQ results in glass models exhibiting considerable differences between the degrees of high- and low-temperature relaxations. For instance, a glass model exhibiting a well-relaxed state at a high-temperature range and a less-relaxed state at a low-temperature range, such as (II-A)900, was obtained using the two-step MQ. In subsequent DMA simulations, this glass model exhibited significant atomic motion at low temperatures and small atomic motion at high temperatures depending on the thermal history of the MQ process. Therefore, the memory effect of

temperature-dependent relaxation can be explained by the existence of different types of relaxations with different characteristic energy barriers. The relaxations with different energy barriers are correlated with the heterogeneous microstructure of the glass solid, as schematically shown in the lower right panel of Fig. 6. The microstructure of glass alloys is heterogeneous in terms of density, atomic mobility, atomic bonding, and local orders. Figures 4(c) and 4(d) show that relaxations with different energy barriers correlate with SBR and WBR, implying that the glass models memorize the spatially heterogeneous relaxation and temperature-dependent relaxation in the preceding MQ process. The unusual energy–structure–property relation is coupled with the memory of the controlled degree of relaxations with different energy barriers in the two-step MQ processes. Additional analyses with respect to MRO [47], the "two order parameters" [48], and other analytical tools can provide further insights on the principles underlying the observed energy–structure–property relation and memory effects, as high- and low-temperature relaxations may have different effects on local orders. This is an interesting topic, which can be investigated in future research.

5. Conclusions

In conclusion, this study focuses on the individual effects of high- and low-temperature relaxations on the properties of metallic glasses. Although both relaxations decrease the potential energy and free volume, unusual energy–structure–property relations were observed to be generated by the controlled high- and low-temperature relaxations; even if the two glass models have similar potential energies, they exhibit different development of local order, elastic stiffness, and plastic deformation behavior. High-temperature relaxation occurring at approximately T_g has a large effect on the formation of local orders. Meanwhile, the low-temperature relaxation as well as the high-temperature relaxation have important effects on the plastic deformation behavior. The temperature-dependent atomic dynamics in the DMA simulations depend on the relaxation histories that occurred in the previous MQ process. This result suggests the memory effect of temperature-dependent relaxation of the previous MQ processes. The different effects of high- and low-relaxations on the potential energy, local orders, elastic stiffness, plastic deformation behavior induce this interesting energy–structure–property relation in glassy states prepared using the two-step MQ processes. The relaxation memory effect can be explained by the existence of relaxations with different energy barriers and heterogeneous microstructures in glassy alloys. These results suggest the possibility of advanced tuning of the energy, structure, and material properties of metallic glasses by controlling the different types of relaxations for material design.

Data availability

The data supporting the findings of this study are available from the corresponding authors upon reasonable request.

Declaration of competing interest

The authors declare that they have no known competing financial interests or personal relationships that could have appeared to influence the work reported in this paper.

Acknowledgements

This study was supported by Grant-in-Aid for Scientific Research (A) (No. 18H03829, No. 23H00228) and Young Scientists (A) (No. 17H04949). Some of the calculations in this study were performed using the Numerical Materials Simulator at the National Institute for Materials Science, Japan.

References

[1] A.L. Greer, Metallic glasses, Science 267 (5206) (1995) pp. 1947-1953. https://doi.org/10.1126/science.267.5206.1947

[2] W.H. Wang, C. Dong, C.H. Shek, Bulk metallic glasses, Mater. Sci. Eng. R Rep. 44 (2-3), (2004) pp. 45-89. https://doi.org/10.1016/j.mser.2004.03.001

[3] J.R. Scully, A. Gebert, J.H. Payer, Corrosion and related mechanical properties of bulk metallic glasses, J. Mater. Res. 22 (2) (2007) pp. 302-313. https://doi.org/10.1557/jmr.2007.0051

[4] M.W. Chen, Mechanical behavior of metallic glasses: Microscopic understanding of strength and ductility, Annu. Rev. Mater. Res. 38 (1) (2008) pp. 445-469. https://doi.org/10.1146/annurev.matsci.38.060407.130226

[5] I.W. Donald, H.A. Davies, Prediction of glass-forming ability for metallic systems, J. Non-Cryst. Solids 30 (1) (1978) pp. 77-85. https://doi.org/10.1016/0022-3093(78)90058-3

[6] P. Chaudhari, D. Turnbull, Structure and properties of metallic glasses, Science 199 (4324) (1978) pp. 11-21. https://doi.org/10.1126/science.199.4324.11

[7] C. Zhang, D. Ouyang, S. Pauly, L. Liu, 3D printing of bulk metallic glasses, Mater. Sci. Eng. R Rep. 145 (2021) Article 100625. https://doi.org/10.1016/j.mser.2021.100625

[8] D.M. Herlach, Non-equilibrium solidification of undercooled metallic melts, Mater. Sci. Eng. R Rep. 4 (2) (1994) pp. 196-234. https://doi.org/10.3390/met4020196

[9] A.I. Taub, F. Spaepen, The kinetics of structural relaxation of a metallic glass, Acta Metall. 28 (12) (1980) pp. 1781-1788. https://doi.org/10.1016/0001-6160(80)90031-0

[10] J.C. Qiao, J.M. Pelletier, Dynamic mechanical relaxation in bulk metallic glasses: A Review, J. Mater. Sci. Technol. 30 (6) (2014) pp. 523-545.

https://doi.org/10.1016/j.jmst.2014.04.018

[11] W.H. Wang, Dynamic relaxations and relaxation-property relationships in metallic glasses, Prog. Mater. Sci. 106 (2019) Article 100561. https://doi.org/10.1016/j.pmatsci.2019.03.006

[12] K.L. Ngai, Z. Wang, X.Q. Gao, H.B. Yu, W.H. Wang, A connection between the structural α-relaxation and the β-relaxation found in bulk metallic glass-formers, J. Chem. Phys. 139 (1) (2013) Article 014502. https://doi.org/10.1063/1.4812281

[13] Q. Wang, S.T. Zhang, Y. Yang, Y.D. Dong, C.T. Liu, J. Lu, Unusual fast secondary relaxation in metallic glass, Nat. Commun. 6 (1) (2015) Article 7876. https://doi.org/10.1038/ncomms8876

[14] F. Zhu, H.K. Nguyen, S.X. Song, Daisman P.B. Aji, A. Hirata, H. Wang, K. Nakajima, M.W. Chen, Intrinsic correlation between β-relaxation and spatial heterogeneity in a metallic glass, Nat. Commun. 7 (1) (2016) Article 11516. https://doi.org/10.1038/ncomms11516

[15] X. Monnier, D. Cangialosi, B. Ruta, R. Busch, I. Gallino, Vitrification decoupling from α-relaxation in a metallic glass, Sci. Adv. 6 (17) (2020) Article eaay1454. https://www.science.org/doi/abs/10.1126/sciadv.aay1454

[16] B. Huang, Z.G. Zhu, T.P. Ge, H.Y. Bai, B.A. Sun, Y. Yang, C.T. Liu, W.H. Wang, Hand in hand evolution of boson heat capacity anomaly and slow β-relaxation in La-based metallic glasses, Acta Mater. 110 (2016) pp. 73-83. https://doi.org/10.1016/j.actamat.2016.03.016

[17] L. Song, W. Xu, J.T. Huo, J.Q. Wang, X. Wang, R. Li, Two-step relaxations in metallic glasses during isothermal annealing, Intermetallics 93 (2018) pp. 101-105. https://doi.org/10.1016/j.intermet.2017.11.016

[18] J. Qian, X.D. Liu, Q. Wang, C. Liu, J. Lu, Y. Yang, Fast secondary relaxation and plasticity initiation in metallic glasses, Natl. Sci. Rev. 5 (5) (2018) pp. 616-618. https://doi.org/10.1093/nsr/nwx113

[19] Y. Liu, H. Bei, C.T. Liu, E.P. George, Cooling-rate induced softening in a $Zr_{50}Cu_{50}$ bulk metallic glass, Appl. Phys. Lett. 90 (7) (2007) 071909. https://doi.org/10.1063/1.2678909

[20] T. Wen, Y. Sun, B. Ye, L. Tang, Z. Yang, K.-M. Ho, C.-Z. Wang, N. Wang, Cooling rate dependence of structural order in $Ni_{62}Nb_{38}$ metallic glass, J. Appl. Phys. 123 (4) (2018) Article 045108. https://doi.org/10.1063/1.5019681

[21] M. Wakeda, J. Saida, Temperature-dependent effect of cooling rate on the melt-quenching process of metallic glasses, Comput. Mater. Sci. 218 (2023) Article 111930. https://doi.org/10.1016/j.commatsci.2022.111930

[22] M. Wakeda, Y. Shibutani, Icosahedral clustering with medium-range order and local elastic properties of amorphous metals, Acta Mater. 58 (11) (2010) pp. 3963-3969.

https://doi.org/10.1016/j.actamat.2010.03.029

[23] M. Wakeda, Y. Shibutani, S. Ogata, J. Park, Relationship between local geometrical factors and mechanical properties for Cu-Zr amorphous alloys, Intermetallics 15 (2) (2007) pp. 139-144. https://doi.org/10.1016/j.intermet.2006.04.002

[24] M. Wakeda, J. Saida, T. Ichitsubo, Atomistic study on simultaneous achievement of partial crystallization and rejuvenated glassy structure in thermal process of metallic glasses, Philos. Mag. 102 (13) (2022) pp. 1209-1230. https://doi.org/10.1080/14786435.2022.2048112

[25] S. Kobayashi, K. Maeda, S. Takeuchi, Computer simulation of deformation of amorphous $Cu_{57}Zr_{43}$, Acta Metall. 28 (12) (1980) pp. 1641-1652. https://doi.org/10.1016/0001-6160(80)90017-6

[26] A.C. Lund, C. Schuh, Yield surface of a simulated metallic glass, Acta Mater. 51 (18) (2003) pp. 5399-5411. https://doi.org/10.1016/S1359-6454(03)00396-3

[27] A.P. Thompson, H.M. Aktulga, R. Berger, D.S. Bolintineanu, W.M. Brown, P.S. Crozier, P.J. in 't Veld, A. Kohlmeyer, S.G. Moore, T.D. Nguyen, R. Shan, M.J. Stevens, J. Tranchida, C. Trott, S.J. Plimpton, LAMMPS -a flexible simulation tool for particle-based materials modeling at the atomic, meso, and continuum scales, Comput. Phys. Commun. 271 (2022) Article 108171. https://doi.org/10.1016/j.cpc.2021.108171

[28] B. Wang, L.J. Wang, W.H. Wang, H.Y. Bai, X.Q. Gao, M.X. Pan, P.F. Guan, Understanding the maximum dynamic heterogeneity during the unfreezing process in metallic glasses, J. Appl. Phys. 121 (17) (2017) Article 175106. https://doi.org/10.1063/1.4982914

[29] H.B. Yu, R. Richert, K. Samwer, Structural rearrangements governing Johari-Goldstein relaxations in metallic glasses, Sci. Adv. 3 (11) (2017) Article e1701577. https://www.science.org/doi/abs/10.1126/sciadv.1701577

[30] H.B. Yu, R. Richert, K. Samwer, Correlation between viscoelastic moduli and atomic ratios in metallic glasses, J. Phys. Chem. Lett. 7 (19) (2016) pp. 3747-3751. https://doi.org/10.1021/acs.jpclett.6b01738

[31] A. Stukowski, Visualization and analysis of atomistic simulation data with OVITO - the Open Visualization Tool, Modell. Simul. Mater. Sci. Eng. 18 (1) (2010) Article 015012. https://dx.doi.org/10.1088/0965-0393/18/1/015012

[32] P.G. Debenedetti, F.H. Stillinger, Supercooled liquids and the glass transition, Nature 410 (6825) (2001) pp. 259-267. https://doi.org/10.1038/35065704

[33] H. Hermann, V. Kokotin, J. Eckert, Locally fluctuating cooling rate as possible reason for non-crystalline plasticity in metallic glasses, EPL, 98 (1) (2012) Article 16003. https://dx.doi.org/10.1209/0295-5075/98/16003

[34] D. Sopu, X. Yuan, J. Eckert, Annealing metallic glasses above T_g in order to accelerate the relaxation process in molecular dynamics simulations, Appl. Phys. Lett. 120 (1) (2022) Article 011904. https://doi.org/10.1063/5.0073204

[35] J. Yu, M. Wang, S. Lin, Slower icosahedral cluster rejuvenation drives the brittle-to-ductile transition in nanoscale metallic glasses, Compu. Mater. Sci. 140 (2017) pp. 235-243. https://doi.org/10.1016/j.commatsci.2017.08.038

[36] P. Kozikowski, M. Ohnuma, R. Hashimoto, K. Takano, G. Herzer, M. Kuhnt, C. Polak, Temperature memory effect of stress annealing-induced anisotropy in metallic glasses, Phys. Rev. Materials 4 (9) (2020) Article 095604. https://link.aps.org/doi/10.1103/PhysRevMaterials.4.095604

[37] M. Wakeda, J. Saida, Heterogeneous structural changes correlated to local atomic order in thermal rejuvenation process of Cu-Zr metallic glass, Sci. Technol. Adv. Mater. 20 (1) (2019) pp. 632-642. https://doi.org/10.1080/14686996.2019.1624140

[38] T. Ichitsubo, E. Matsubara, T. Yamamoto, H.S. Chen, N. Nishiyama, J. Saida, K. Anazawa, Microstructure of fragile metallic glasses inferred from ultrasound-accelerated crystallization in Pd-based metallic glasses, Phys. Rev. Lett. 95 (24) (2005) Article 245501. https://link.aps.org/doi/10.1103/PhysRevLett.95.245501

[39] T. Ichitsubo, S. Hosokawa, K. Matsuda, E. Matsubara, N. Nishiyama, S. Tsutsui, A.Q.R. Baron, Nanoscale elastic inhomogeneity of a Pd-based metallic glass: Sound velocity from ultrasonic and inelastic X-ray scattering experiments, Phys. Rev. B 76 (14) (2007) Article 140201(R). https://link.aps.org/doi/10.1103/PhysRevB.76.140201

[40] J. Hachenberg, D. Bedorf, K. Samwer, R. Richert, A. Kahl, M.D. Demetriou, W.L. Johnson, Merging of the α and β relaxations and aging via the Johari-Goldstein modes in rapidly quenched metallic glasses, Appl. Phys. Lett. 92 (13) (2008) Article 131911. https://doi.org/10.1063/1.2903697

[41] H.B. Yu, W.H. Wang, H.Y. Bai, Y. Wu, M.W. Chen, Relating activation of shear transformation zones to β relaxations in metallic glasses, Phys. Rev. B 81 (22) (2010) Article 220201. https://link.aps.org/doi/10.1103/PhysRevB.81.220201

[42] T.J. Lei, L. Rangel DaCosta, M. Liu, W.H. Wang, Y.H. Sun, A.L. Greer, M. Atzmon, Shear transformation zone analysis of anelastic relaxation of a metallic glass reveals distinct properties of α and β relaxations, Phys. Rev. B 100 (2) (2019) Article 033001. https://link.aps.org/doi/10.1103/PhysRevE.100.033001

[43] Z.Y. Zhou, Q. Chen, Y. Sun, H.B. Yu, Unveiling correlation between α_2 relaxation and yielding behavior in metallic glasses, Phys. Rev. B 103 (2021) Article 094117. https://doi.org/10.1103/PhysRevB.103.094117

[44] S.Y. Zhang, W.H. Zhou, L.J. Song, J.T. Huo, J.H. Yao, J.Q. Wang, Y. Li, Decoupling

between enthalpy and mechanical properties in rejuvenated metallic glass, Scr. Mater. 223 (2023) Article 115056. https://doi.org/10.1016/j.scriptamat.2022.115056

[45] M. Gao, J.H. Perepezko, Separating β relaxation from α relaxation in fragile metallic glasses based on ultrafast flash differential scanning calorimetry, Phys. Rev. Materials 4 (2) (2020) Article 025602. https://link.aps.org/doi/10.1103/PhysRevMaterials.4.025602

[46] K. Geirhos, P. Lunkenheimer, A. Loidl, Johari-Goldstein relaxation far below T_g: Experimental evidence for the Gardner transition in structural glasses? Phys. Rev. Lett. 120 (8) (2018) Article 085705. https://link.aps.org/doi/10.1103/PhysReLett.120.085705

[47] Z.W. Wu, M.Z. Li, M. Liu, W.H. Wang, K.X. Liu, Correlation between structural relaxation and connectivity of icosahedral clusters in CuZr metallic glass-forming liquids, Phys. Rev. B 88 (5) (2013) Article 054202. https://doi.org/10.1103/PhysRevB.88.054202

[48] H. Tanaka, Bond orientational order in liquids: Towards a unified description of water-like anomalies, liquid-liquid transition, glass transition, and crystallization, Eur. Phys. J. E 35 (2012) Article 113. https://doi.org/10.1140/epje/i2012-12113-y

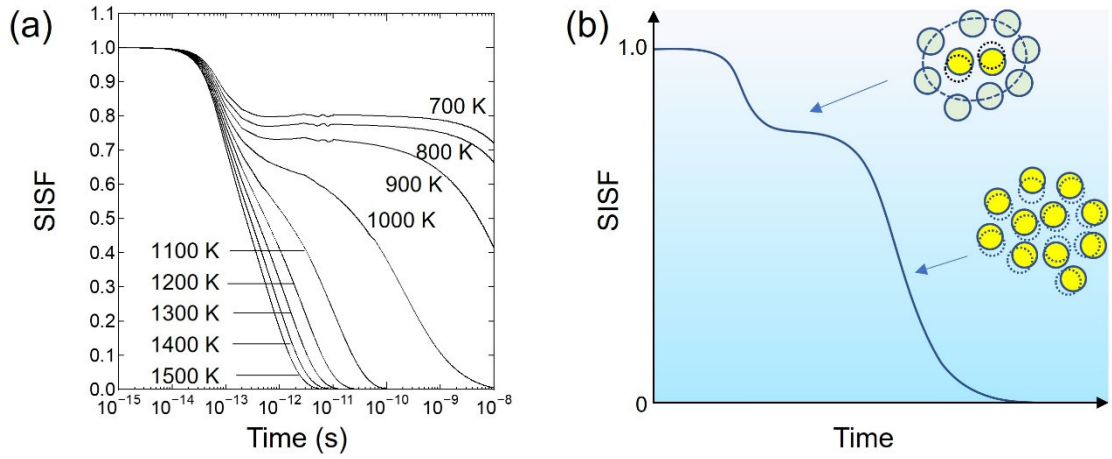

Fig. 1. Self-intermediate scattering function (SISF) vs. time. (a) SISF of the present model system at various temperatures. At each temperature, we conducted independent simulations with different initial atomic configurations and took the statistical average of the calculated SISFs. (b) Schematic of the two-stage reduction of the SISF and related atomic dynamics.

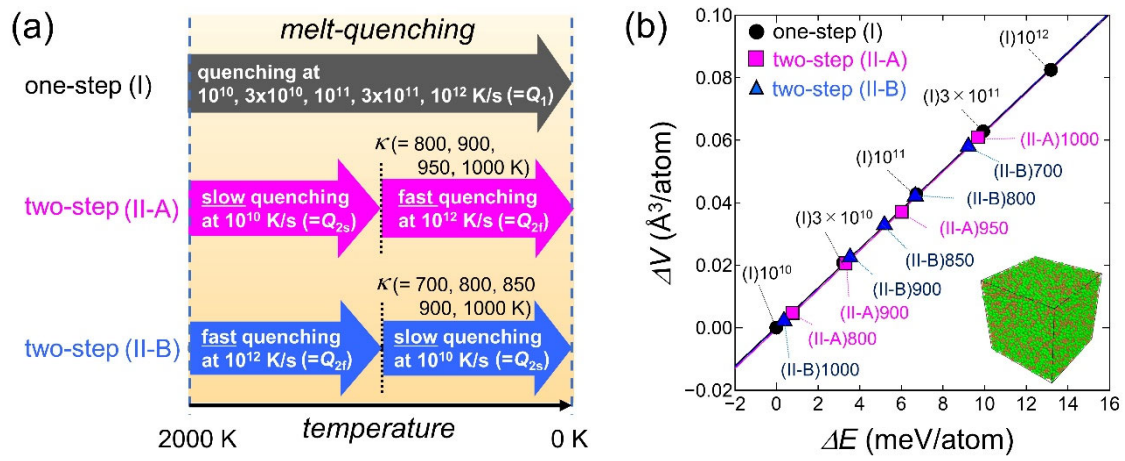

Fig. 2. Melt-quenching (MQ) simulations and obtained potential energy–volume correlation. (a) Schematic of one-step and two-step MQ processes; two-step (II-A) involves slow to fast quenching, and two-step (II-B) involves fast to slow quenching. (b) Volume vs. potential energy correlation at 0 K obtained by one-step and two-step MQ processes. The potential energies and volumes per atom are shown as the differentiated value from one-step MQ model, (I)10^{10}, which has the lowest potential energy and volume among all models. The temperature values in panel (b) represent κ (i.e., the temperature at which the cooling rate changes in two-step MQ processes). The three lines in panel (b) show the mean-square fitting for one-step, two-step (II-A), and two-step (II-B) MQ processes (the three lines are almost identical). An atomic model constructed by MQ process is embedded in panel (b).

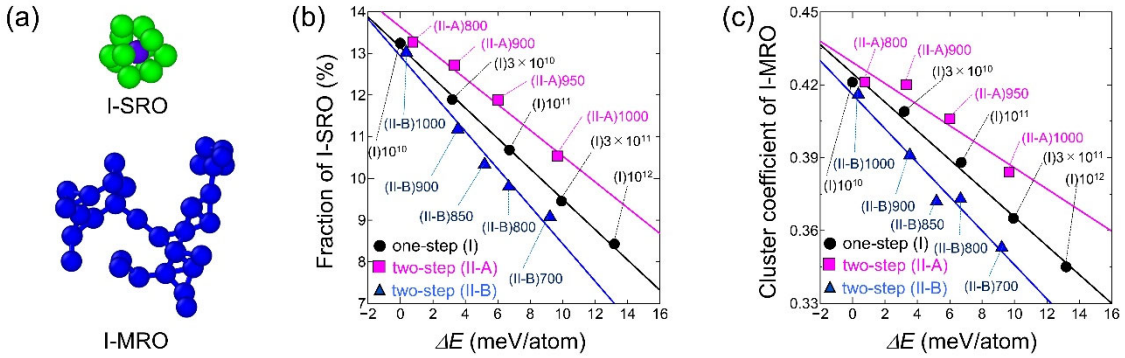

Fig. 3. Relationship between internal structure and potential energy. (a) Examples of observed I-SRO (the blue atom is a center atom, and green atoms are 12 surrounding atoms) and I-MRO composed of 34 I-SRO (only center atoms of I-SRO are shown). For I-MRO, we also show the atomic bonding between the center atoms of I-SRO, which are used for clustering-coefficient analysis. [22] (b) Fraction of I-SRO and (c) clustering coefficient of I-MRO vs. potential energy. In panels (b) and (c), the potential energies are shown as the differentiated value from the one-step MQ model with $Q_1 = 10^{10}$ K/s (i.e., (I)10^{10}).

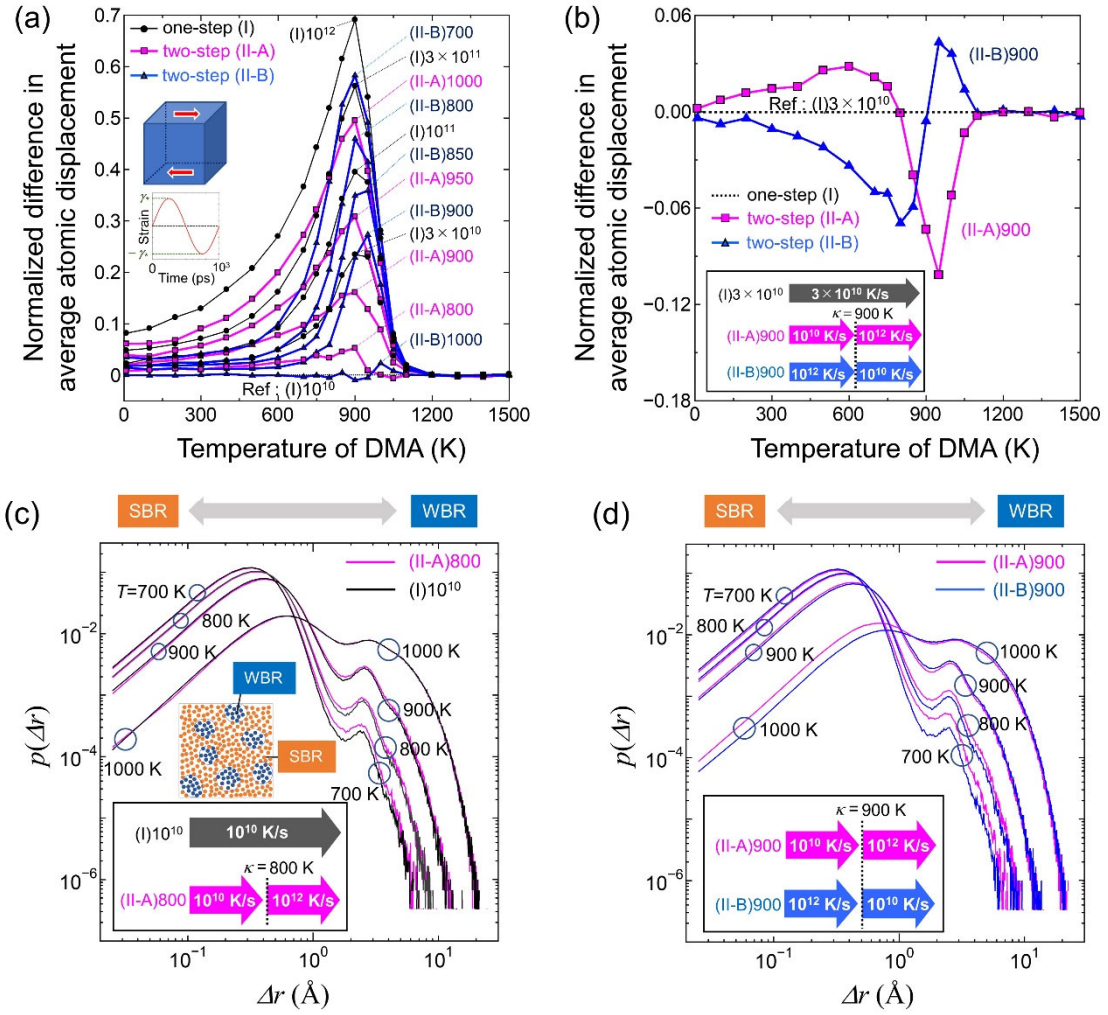

Fig. 4. Dynamic behavior evaluated by DMA at various temperatures. (a) Average atomic displacement vs. temperature from 10 K to 1500 K. For each model named X and temperature T, we conducted DMA simulations and evaluated the normalized average atomic displacement $\overline{\Delta r}[X,T]$ within one period of DMA simulations. The vertical axis is calculated using $\{\overline{\Delta r}[X,T]$-$\overline{\Delta r}[(\mathrm{I})10^{10},T]\}/\overline{\Delta r}[(\mathrm{I})10^{10},T]$, i.e., it represents the normalized difference between a model X and $(\mathrm{I})10^{10}$, which has the lowest potential energy and volume among all models. The embedded images schematically show the DMA simulation settings of strain direction and strain time evolution. (b) The difference in the average atomic displacement between (II-A)900 and (I)3 × 10^{10}, or (II-B)900 and (I)3 × 10^{10} normalized by $(\mathrm{I})10^{10}$; these value are calculated using $\{\overline{\Delta r}[(\mathrm{II}$-$\mathrm{A})900,T]$-$\overline{\Delta r}[(\mathrm{I})3 \times 10^{10},T]\}/\overline{\Delta r}[(\mathrm{I})10^{10},T]$ or $\{\overline{\Delta r}[(\mathrm{II}$-$\mathrm{B})900,T]$-$\overline{\Delta r}[(\mathrm{I})3 \times 10^{10},T]\}/\overline{\Delta r}[(\mathrm{I})10^{10},T]$, respectively. Histograms of atomic displacement, Δr, at 700, 800, 900, and 1000 K; (c) (II-A)800 vs. $(\mathrm{I})10^{10}$ and (d) (II-A)900 vs. (II-B)900.

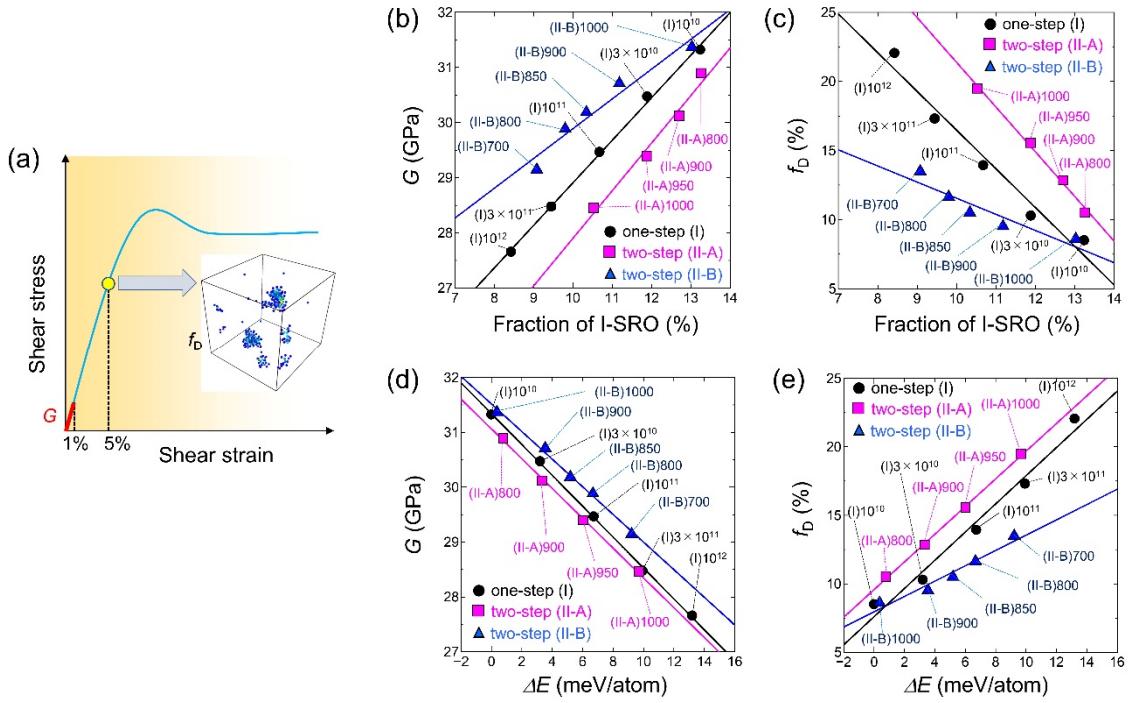

Fig. 5. Elastic stiffness and plastic deformation behavior obtained by shear simulations. (a) Schematic of shear stress vs. strain relation; the definitions of shear stiffness G and deformation ratio f_D are shown. (b) and (c) are G and f_D vs. fraction of I-SRO, respectively. (d) and (e) are G and f_D vs. potential energy, respectively. In panels (d) and (e), the potential energies (i.e., the horizontal axis) are shown as the differentiated value from one-step MQ model with $Q_1 = 10^{10}$ K/s (i.e., (I)10^{10}).

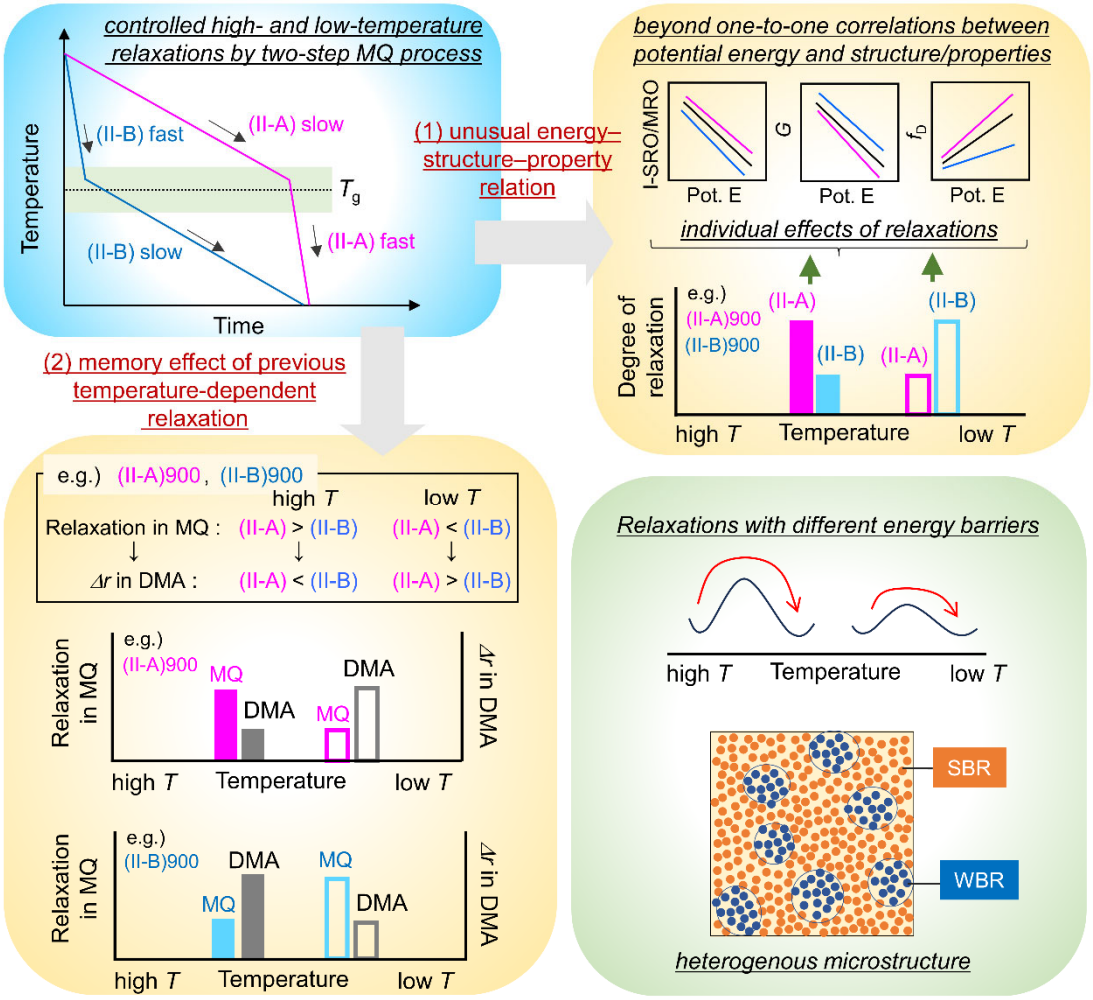

Fig. 6. Schematic explanation of the unusual energy–structure–property relationship and the relaxation memory effects. The upper left image shows the two-step MQ processes used to control high- and low-temperature relaxations, and the upper right image shows the unusual energy–structure–property relation induced by controlling the high- and low-temperature relaxations. The lower figures explain the relaxation memory effect observed in DMA simulations. The memory effect is caused by the relaxations with different energy barriers and by the spatially heterogeneous relaxations in the heterogeneous microstructure with SBR and WBR.